Available online at www.sciencedirect.com

ScienceDirect

Procedia CIRP 126 (2024) 1047–1052

www.elsevier.com/locate/procedia

17th CIRP Conference on Intelligent Computation in Manufacturing Engineering (CIRP ICME '23)

Experimental validation of the plane-based penetration calculation for the gear skiving of internal gears

Charalampos Alexopoulos[a,*], Christopher Janßen[a], Mareike Solf[a], Thomas Bergs[a,b]

[a]WZL of RWTH Aachen University, Campus-Boulevard 30, 52074 Aachen, Germany
[b]Fraunhofer IPT, Steinbachstraße 17, 52074 Aachen

* Corresponding author. Tel.: +49-241-80-27366; *E-mail address:* c.alexopoulos@wzl.rwth-aachen.de

Abstract

Gear skiving is a flexible and productive process for the manufacturing of internal and external gears. Due to the variable cutting conditions and the complex process kinematics, a simulative investigation of the skiving process is necessary for an efficient and economic process design. The plane-based penetration calculation is an established method for simulating the machining of gears. In this paper, this simulation approach is validated based on experimental results for the gear skiving process of internal gears. For almost all simulation results, the results of the gear skiving simulation for internal gears agreed with the experimental results.

© 2024 The Authors. Published by Elsevier B.V.
This is an open access article under the CC BY-NC-ND license (https://creativecommons.org/licenses/by-nc-nd/4.0)
Peer-review under responsibility of the scientific committee of the 17th CIRP Conference on Intelligent Computation in Manufacturing Engineering (CIRP ICME'23)

Keywords: Gear skiving; Internal gears; Simulation; validation

1. Introduction and motivation

Gear skiving is a flexible and productive process for the manufacturing of gears. The process can be used both for the manufacturing of internal and external gears. It is an advantageous alternative for the production of internal gears due to its higher productivity compared to shaping and higher flexibility compared to broaching [1]. Gear skiving can also be used for the manufacturing of external gears, in the case of internal and external gears are to be produced on a component in a single clamping operation or if interference prevents production by hobbing.

Due to the variable cutting conditions and the complex process kinematics, a simulative investigation of the skiving process is necessary for an efficient and economic process design. With a plane-based penetration calculation, process characteristics can be determined [2, 3]. These include, among others, the undeformed chip thickness, chip volume and maximum undeformed chip length. Furthermore, three-dimensional chips can be extracted.

The skiving simulation SPARTAPRO, which use the plane-based penetration calculation, has already been successfully validated for external gears. Further validation for the simulation of internal gears is required and will be conducted within the scope of this study. To this end, simulation results will be compared to experimental ones and their agreement or correlation will be investigated.

2. State of the art

In the skiving process, the tool rotation axis is inclined with respect to the workpiece rotation axis by a cross-axis angle Σ. The cross-axis angle Σ results from the sum of the workpiece helix angle β_2 and the tool helix angle β_0 [4]. The rotational motion of the tool combined with the cross-axis angle Σ leads to a relative motion along the workpiece flank. In addition, the

2212-8271 © 2024 The Authors. Published by Elsevier B.V.
This is an open access article under the CC BY-NC-ND license (https://creativecommons.org/licenses/by-nc-nd/4.0)
Peer-review under responsibility of the scientific committee of the 17th CIRP Conference on Intelligent Computation in Manufacturing Engineering (CIRP ICME'23)
10.1016/j.procir.2024.09.001

rotational motion of the tool is superimposed by an axial feed f_a parallel to the workpiece rotational axis [5].

The simulation of a manufacturing process is important for economic process design. Simulated process characteristics can be used to gain a deeper insight into the machining conditions [6]. In this way, process and tool parameters can be optimized prior to manufacturing and thus reducing the need of lengthy trials [7].

The plane-based penetration calculation is an established method for simulating the machining of gears [8–12]. The scope of the program is shown in Fig. 1. Tool and workpiece geometry as well as kinematic and process data are the necessary input data of the simulation. Both, the workpiece and the tool envelope are discretized in sectional planes. After the tool and the workpiece have been set up, they are positioned relative to each other. Taking into account the process-specific kinematics, the tool profile penetrates the workpiece. The sectional planes of the tool envelope are projected onto the planes of the workpiece. If there is a superposition, the common cutting surface is determined. After evaluating the cutting surfaces for each cut, the results are displayed [8, 13, 14]. Those regard the chip and workpiece geometry as well as the process characteristic values.

Fig. 1. Scope of services of SPARTAPRO

Output of the plane-based penetration calculation is the geometry of the undeformed chips, as their deformation isn't taken into account. A model has been developed by KRÖMER [7] for the simulation of chip deformation for gear hobbing. Each simulated chip can be output as a three-dimensional body and saved in the VISUALIZATION TOOLKITS (VTK) data format. This file contains information regarding the locally and temporally resolved chip thickness h_{cu} as well as the position and direction of the tool cutting edge at each point. This information is read and processed in a post-processor. This post-processor divides each chip into individual fragments, which are deformed independently of each other, and then follows the calculation scheme shown in Fig. 2 [7].

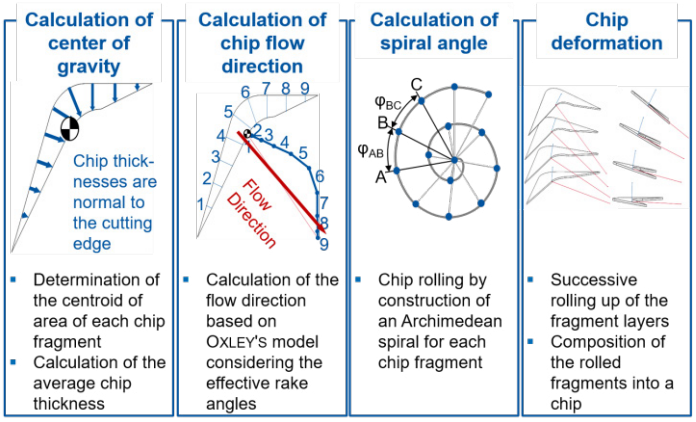

Fig. 2. Principle of chip deformation simulation [7]

Initially, the center of gravity of each fragment in all chip planes and the average chip thickness in each of these planes are determined. The chip flow direction is determined using the extended model according to OXLEY [15] . For this purpose, the vectors of the tool normals from the VTK file are added, taking into account the effective rake angles. The rolling up of the chip is described by constructing an Archimedean spiral for each fragment. To this end, the spiral angle is calculated.

The fragment layers are then successively rolled up and finally, the rolled fragments are assembled to form a chip. To avoid kinks at the transition points, the assembly of the individual spiral elements takes place with a tangential transition. For the validation of this model, both KRÖMER and BERGS performed fly-cutting trials on gear hobbing and the simulated chips were compared with the manufactured ones [7, 16]. By using a fly cutter instead of a solid tool, a single chip is produced per tool revolution, which allowed the targeted observation of specific chips for the validation.

3. Objective and approach

The validation of the plane-based penetration calculation for skiving of internal gears is carried out in three steps (see Fig. 3). First, the influence of the axial feed f_a on the flank topography is investigated. Different axial feeds f_a are selected and the height of the feed marks δ_x is determined by simulation. Internal gears are manufactured and the resulting tooth flank topography is measured. The simulated tooth flank topography and the height of the feed marks are then compared to the measured values.

Simulated chip characteristics can be interpreted as a mechanical load on the tool and thus provide an indication of the expected tool wear [17]. In the next step, chip characteristics (maximum chip thickness $h_{cu,max}$) are calculated for two different process and workpiece designs and compared with experimentally determined tool wear. Finally, conclusions are drawn regarding a possible correlation.

In addition, the chip deformation is calculated using the KRÖMER method and the simulated chip geometry is compared

with manufactured chips. This verifies whether the simulated chip geometries are plausible.

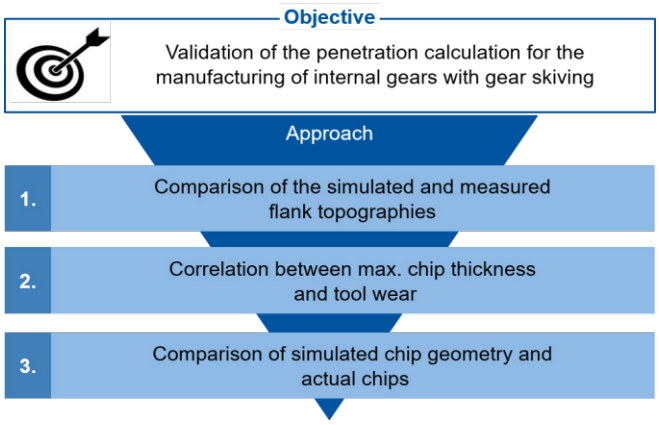

Fig. 3. Objective and approach

4. Simulation and experimental setup

This chapter regards the simulation and experimental setup. Two process and workpiece designs are considered for the investigations. Workpiece and tool geometry as well as kinematic and process data represent the necessary input data for the simulation. The workpiece, tool and process data are shown in Fig. 4.

Fig. 4. Workpiece, tool and process data

The workpiece gear A was an internal gear with a module of $m_{n2} = 2.97$ mm, $z_2 = -85$ teeth, a pressure angle of $a_{n2} = 25°$ and a helix angle of $\beta_2 = 0°$. The gear width was $b_2 = 45$ mm. The tool used to manufacture the gear A was a skiving tool with a module $m_{n0} = 2.97$ mm and a number of teeth $z_0 = 51$. The helix angle of the tool was $\beta_0 = 20°$. The gear was produced in N = 15 cuts and the cutting speed was $v_c = 90$ m/min. The axial feed varied between values from $f_a = 1$ mm and $f_a = 1.7$ mm in order to keep the maximum chip thickness $h_{cu,max}$ constant throughout the process.

The gear case B was also an internal spur gear with module of $m_{n2} = 3.2$ mm, number of teeth $z_2 = -90$ and pressure angle of $\alpha_{n2} = 20°$. The tool had the same normal module as the gear, while the helix angle was $\beta_2 = 20°$. The machining was performed in 15 cuts (N = 15) and with a cutting speed of $v_c = 90$ m/min. The axial feed was $f_a = 1$ mm to $f_a = 1.5$ mm.

The experimental investigations were carried out on a GLEASON-PFAUTER 300PS gear skiving machine using FUCHS ECOCUT coolant. The clamping systems used were inspected for radial and axial runout prior testing. The gears were then measured on a KLINGELNBERG P65 gear measuring machine. During the topography measurement, 50 profile lines and 200 flank lines were evaluated.

The tools used were made of powder metallurgical high-speed steel (PM-HSS) grade S390 and were inspected for possible damage using a KEYENCE digital microscope before the test was carried out. The tools were coated with an AlCrN coating. During the test, the same cutting conditions were set as in the simulation. After the test, the tool wear was evaluated using the microscope.

5. Validation of the plane-based penetration calculation

The following subsections describe the steps required to validate the plane-based penetration calculation. The validation is performed in three steps. First, the simulated and measured flank topographies are analyzed. In the second step, the calculated max chip thickness $h_{cu,max}$ is compared to the tool wear. Finally, simulated chips are compared with manufactured chips.

5.1. Comparison of the simulated and measured flank topographies

Feed marks occur by the continuous axial feed as the workpiece rotates. The feed mark depth δ_x varies with the amount of axial feed f_a. To reduce the feed mark depth and the mechanical stress on the tool, the axial feed is often reduced. In this report, the relationship between axial feed and feed mark depth is first investigated simulatively (see Fig. 5). Subsequently, the simulated flank topographies are compared with experimentally evaluated topographies for two different values of axial feed f_a.

A representative gear gap is shown at the top left of Fig. 5. Manufacturing deviations can be seen in the form of a waviness on the tooth flank. The distance between the peaks corresponds to the amount of axial feed f_a. To calculate the height of the feed marks δ_x, the gear gap geometries for the three axial feed variants ($f_a = 1.5$ mm, $f_a = 2.5$ mm, $f_a = 5$ mm) are simulated and compared with an ideal gap geometry. In the ideal gap geometry, no manufacturing deviations are present. The height of the feed marks δ_x is shown in the diagrams.

From Fig. 5 it can be concluded that the number of local maxima decreases as the axial feed f_a increases. In addition, multiplying the number of local maxima by the amount of axial feed is consistent with the gear width b_2 in all three cases considered. Furthermore, it can be seen that the height of the feed marks can be reduced at smaller feed. For an axial feed of $f_a = 5$ mm, the height of the feed marks was $\delta_x = 80$ µm, while

a feed of $f_a = 2.5$ mm resulted in a value of $\delta_x = 12$ µm. The smallest feed mark depth was observed at $f_a = 1.5$ mm and was determined at $\delta_x = 6$ µm.

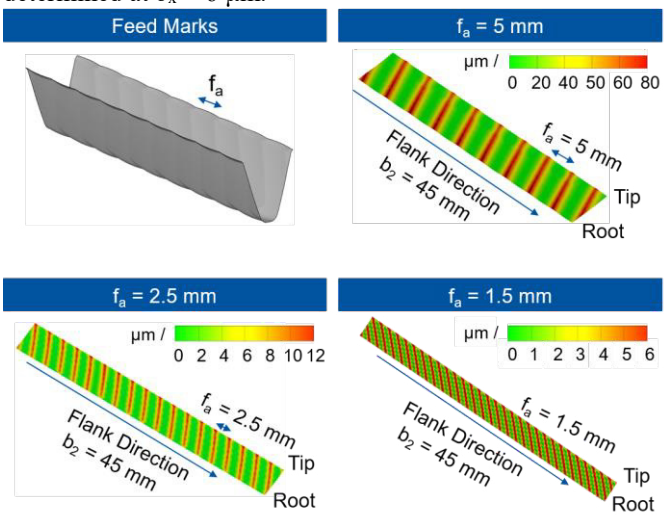

Fig. 5. Simulated flank topographies for different values of axial feed f_a

The upper part of Fig. 6. depicts the simulated topographies, while the lower part shows the measured ones. The comparison was made on the same section of the tooth flank. The experimentally determined feed mark depth at a feed of $f_a = 1$ mm was $\delta_x = 3.5$ µm, while the simulated feed mark depth was $\delta_x = 4$ µm. For the axial feed of $f_a = 1.5$ mm, feed mark depths of $\delta_x = 6$ µm were measured. Simulatively, these amounted also to $\delta_x = 6$ µm. It can be concluded that a very good agreement was obtained between the simulated and the measured flank topographies.

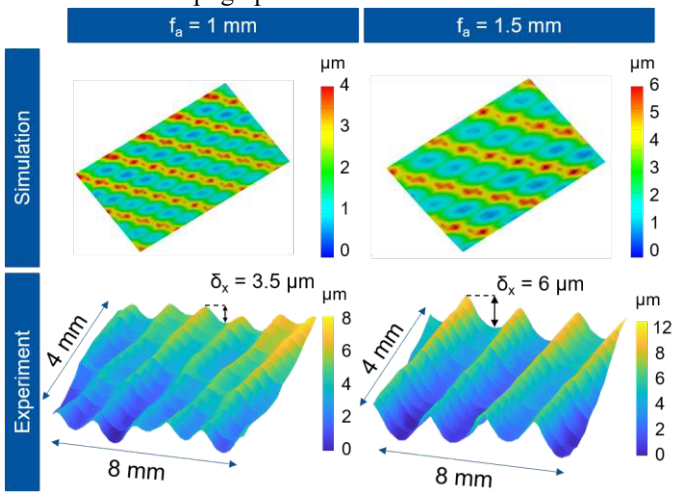

Fig. 6. Comparison of simulated and measured flank topographies

5.2. Correlation between max. chip thickness $h_{cu,max}$ and tool wear

A comparison of the max. chip thickness $h_{cu,max}$ over the tool profile and the tool wear is shown in Fig. 7 for the manufacturing of gear A. On the left, the curves of the maximum chip thickness $h_{cu,max}$ are presented. On the right, the rake face and the tip of a slightly worn tool are depicted.

It is expected that the amount of wear occurring correlates to the simulated local chip thickness. This assumption is confirmed by the comparison presented on Fig. 7. The wear images show that the rake face is discoloured along the entire cutting edge. In the simulation results, chip thickness variations were observed along the trailing flank (TF) and leading flank (LF). The discolouration of the rake face is more pronounced at the tip of the tool, which agrees well with the curves of the max. chip thickness $h_{cu,max}$. Therefore, it can be concluded that the simulation and the trial represent the same contact area.

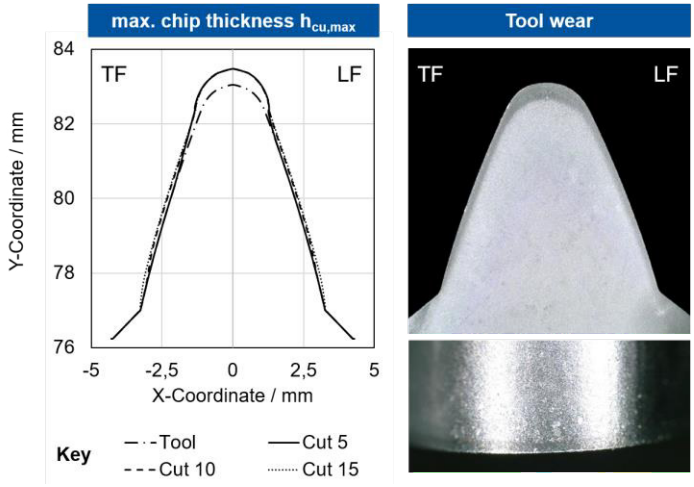

Fig. 7. Comparison of max. chip thickness $h_{cu,max}$ and tool wear - Gear A

Tool wear images of the rake face and of the tool tip at the end of tool life from the manufacturing of gear B as well as the max. chip thickness $h_{cu,max}$ over the tool profile are shown in Fig. 8.

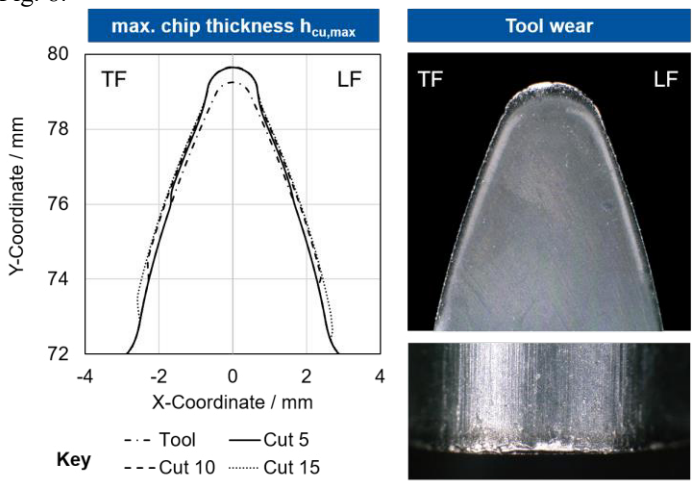

Fig. 8. Comparison of max. chip thickness $h_{cu,max}$ and tool wear - Gear B

Again, the wear is clearly more pronounced at the tip than on the flank. In addition, the discoloration and the wear on the

rake face were more evident on the trailing flank compared to the leading flank. An observation of the max. chip thickness $h_{cu,max}$ (see Fig. 8) shows higher values on the trailing flank, accompanied by discolouration of the rake face. However, course of the max. chip thickness $h_{cu,max}$ is slightly shifted to the left, which is not visible on the wear pattern.

5.3. Comparison of simulated chip geometry to manufactured chips

In this chapter the simulated undeformed chip geometry, the deformed chip geometry and the geometry of the manufactured chips are compared. For this purpose, undeformed chip geometries are calculated by the plane-based penetration calculation. In order to simulate the deformed chip geometry, the model according to KRÖMER [7] is used. Finally, manufactured chips are collected and are compared to the simulated ones.

Chip geometries were simulated for each cut. Fig. 9 shows the results for two cuts as an example and concerns twisted and double-flanked chips (V-chips) from the manufacturing of gear A. Both, the simulative and the experimental investigation have shown that double-flanked chips occur from the fifth cut onwards. In the fourth and tenth cut, the chip thicknesses were $h_{cu,max}$ = 0.22 mm and $h_{cu,max}$ = 0.21 mm, respectively.

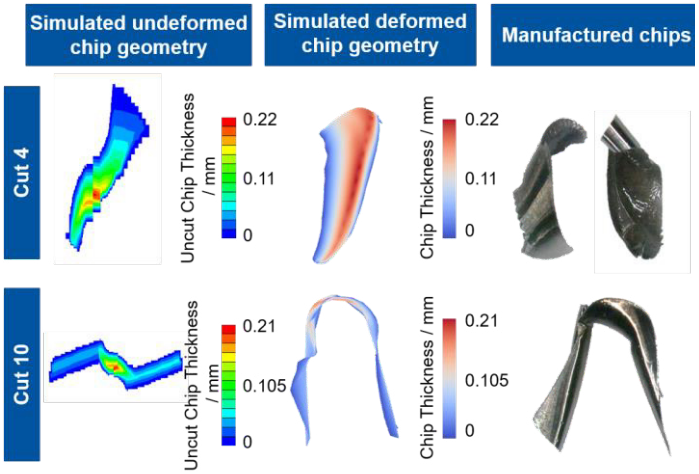

Fig. 9. Comparison of simulated and manufactured chip geometries - Gear A

Afterwards, the simulated chip geometry was imported into post-processor for deforming the chips. The deformed chips are shown in the center of Fig. 9. By comparing the simulated deformed chips with the experimentally determined chip geometry for cuts four and ten, it can be seen that simulated and experimental results are very close to each other. The same investigation was also carried out for gear B.

Similar results regarding the chip form as for the manufacturing of gear A were also obtained by the manufacturing of gear B (see Fig. 10). For cut 10, the comparison between simulated and experimentally determined chip shapes showed very good agreement. For the fourth cut, similarities were observed between simulation and experiment, but larger discrepancies were observed between the chip shapes. This discrepancy could be caused by the influence of temperature on the chip deformation of the manufactured chips.

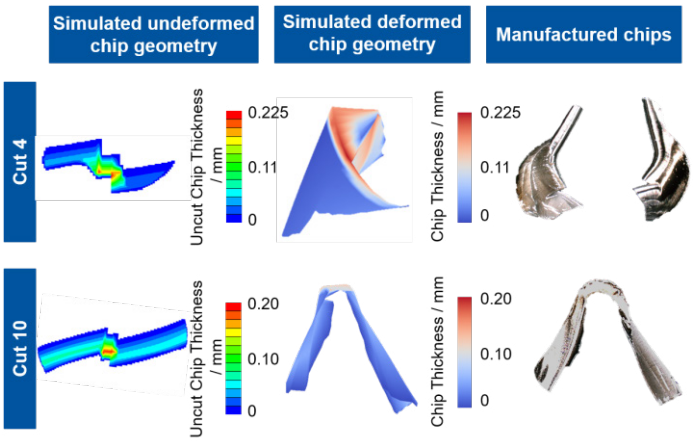

Fig. 10. Comparison of simulated and manufactured chip geometries - Gear B

6. Summary and outlook

Due to the variable cutting conditions and the complex process kinematics, a simulative investigation of the skiving process is necessary for an efficient and economic process design. With on a plane-based penetration calculation, process characteristics can be determined. These include, among others, the undeformed chip thickness, chip volume and maximum undeformed chip length. Furthermore, three-dimensional chips can be extracted. The skiving simulation SPARTAPRO, which use the plane-based penetration calculation, has already been successfully validated for the simulation of external gears. Further validation of the plane-based penetration calculation, for simulating the gear skiving process of internal gears, has been conducted within the scope of this study. For almost all findings, the results of the gear skiving simulation for internal gears agreed with the experimental results.

In this paper, simulated and measured flank topographies were compared under different process conditions and the influence of the axial feed on the tooth flank topography was determined both simulatively and experimentally. In addition, chip characteristics were compared with tool wear behavior for two different process and workpiece designs, and their correlations were investigated. Furthermore, uncut chip geometries were extracted from the plane-based penetration calculation. Those were then deformed using a post-processor and compared to the manufactured chips, which were collected during the trials.

For almost all simulation results, it could be shown that the results of the plane-based penetration calculation for skiving of internal gears agreed with the experimental results. Based on the results, it can be concluded, that the plane-based penetration calculation has been successfully evaluated also for the case of internal gears.

By an observation of the max. chip thickness $h_{cu,max}$, and the tool wear behavior, it was found that in both process and workpiece designs (A and B), the tip of the tool has been experiencing greater mechanical loads in comparison to the flanks and consequently exhibited the highest wear. An optimization possibility at this point would be to reduce the axial feed f_a in order to reduce the maximum chip thicknesses. However, such an adjustment of the process design is accompanied by an increase in process time and cutting length, which will possibly increase the tool wear.

In order to extend the validation of the plane-based penetration calculation, the skiving simulation will be validated on additional application cases in the future. Gear designs with helix angles will be simulated and the results will be compared to experimental ones.

Acknowledgements

The authors gratefully acknowledge financial support by the WZL Gear Research Circle for the achievement of the project results.

References

[1] Z. Ren *et al.,* "Parametric modeling of uncut chip geometry for predicting crater wear in gear skiving," *Journal of Materials Processing Technology*, vol. 290, p. 116973, 2021, doi: 10.1016/j.jmatprotec.2020.116973.

[2] A. Bechle, "Beitrag zur prozesssicheren Bearbeitung beim Hochleistungsfertigungsverfahren Wälzschälen," Diss., wbk Institut für Produktionstechnik der Universität Karlsruhe, Universität Karlsruhe, Karlsruhe, 2006.

[3] A. Marinakis, P. Alevras, and A. Antoniadis, "A systematic analysis of the power skiving process using a novel gear manufacturing simulation software," *Simulation Modelling Practice and Theory*, vol. 123, p. 102711, 2023, doi: 10.1016/j.simpat.2022.102711.

[4] R. Bauer, "Modellbasierte Auslegung von Mehrschnittstrategien beim Wälzschälen," Diss., Fraunhofer IWU, Technische Universität Chemnitz, Chemnitz, 2018.

[5] F. Klocke, C. Brecher, C. Löpenhaus, and J. Mazak, "Describing and Evaluating Deviations for Bevel Gear Flanks," *Procedia CIRP*, vol. 62, pp. 221–226, 2017, doi: 10.1016/j.procir.2016.06.045.

[6] O. Winkel, "Steigerung der Leistungsfähigkeit von Hartmetallwälzfräsern durch eine optimierte Werkzeuggestaltung," Diss., Werkzeugmaschinenlabor (WZL) der RWTH Aachen, RWTH Aachen University, Aachen, 2005.

[7] M. Krömer, "Entstehung von Spanaufschweißungen beim Trockenwälzfräsen," Diss., RWTH Aachen, Aachen, 2019.

[8] C. Janßen, J. Brimmers, and T. Bergs, "Validation of the plane-based penetration calculation for gear skiving," *Procedia CIRP*, vol. 99, pp. 220–225, 2021, doi: 10.1016/j.procir.2021.03.034.

[9] J. Mazak, F. Klocke, T. Bergs, C. Brecher, and C. Löpenhaus, "Simulation-Based Process Analysis for Discontinuous Cutting of Generated Bevel Gears," *Proc. Inst. Mech. Eng. Part C: J. Mech. Eng. Sci.*, vol. 233, 21-22, pp. 7378–7390, 2019.

[10] B. Vargas, M. Zapf, J. Klose, F. Zanger, and V. Schulze, "Numerical Modelling of Cutting Forces in Gear Skiving," *Procedia CIRP*, vol. 82, pp. 455–460, 2019, doi: 10.1016/j.procir.2019.04.039.

[11] F. Klocke, C. Brecher, C. Löpenhaus, and M. Krömer, "Calculating the Workpiece Quality Using a Hobbing Simulation," *Procedia CIRP*, vol. 41, pp. 687–691, 2016, doi: 10.1016/j.procir.2015.12.045.

[12] K.-D. Bouzakis, "Konzept und technologische Grundlagen zur automatisierten Erstellung optimaler Bearbeitungsdaten beim Wälzfräsen," Habil.-Schr., Werkzeugmaschinenlabor (WZL) der RWTH Aachen, RWTH Aachen University, Aachen, 1981.

[13] F. Klocke and C. Brecher, *Zahnrad- und Getriebetechnik: Auslegung - Herstellung - Untersuchung - Simulation*. München: Carl Hanser Verlag, 2017.

[14] F. Klocke and W. König, *Fertigungsverfahren 1: Drehen, Fräsen, Bohren,* 8th ed. Berlin: Springer, 2008.

[15] P. L. B. Oxley and M. C. Shaw, "Mechanics of Machining: An Analytical Approach to Assessing Machinability," *Journal of Applied Mechanics*, vol. 57, no. 1, p. 253, 1990, doi: 10.1115/1.2888318.

[16] T. Bergs, J. Brimmers, A. Georgoussis, and M. Krömer, "Investigation of the chip formation during hobbing by means of an analytical approach," *Procedia CIRP*, vol. 99, pp. 226–231, 2021, doi: 10.1016/j.procir.2021.03.033.

[17] A. Mundt, "Modell zur rechnerischen standzeitbestimmung beim Wälzfräsen," Diss., Werkzeugmaschinenlabor (WZL) der RWTH Aachen;, RWTH Aachen University, Aachen, 1992.